Spin-Peierls distortions in $TiPO_4$

Maxim Bykov,[1] Jian Zhang,[1] Andreas Schönleber,[1] Alexander Wölfel,[1] Sk Imran Ali,[1] Sander van Smaalen,[1,*] R. Glaum,[2] H.-J. Koo,[3] M.-H. Whangbo,[4] P. G. Reuvekamp,[5] J. M. Law,[5] C. Hoch,[5] and R. K. Kremer[5]

[1]*Laboratory of Crystallography, University of Bayreuth, 95440 Bayreuth, Germany*

[2]*Institute of Inorganic Chemistry, University of Bonn, 53121 Bonn, Germany*

[3]*Department of Chemistry and Research Institute for Basic Sciences, Kyung Hee University, Seoul 130-701, Republic of Korea*

[4]*Department of Chemistry, North Carolina State University, Raleigh, North Carolina 27695, USA*

[5]*Max Planck Institute for Solid State Research, 70569 Stuttgart, Germany*

(Received 20 July 2013; revised manuscript received 2 November 2013; published 19 November 2013)

On the basis of single-crystal x-ray diffraction we show that $TiPO_4$ undergoes a spin-Peierls distortion below 74.5(5) K, with a dimerization of the Ti chains along the **c** axis. Between 74.5(5) and 111.6(3) K, $TiPO_4$ develops an incommensurate (IC) phase with temperature-dependent **q** vector (σ_1,0,0). Density functional calculations strongly suggest that the IC phase results from a frustration of the lock-in spin-Peierls transition due to the competition of three energetically almost degenerate crystal structures and elastic coupling of the Ti chains via the bridging PO_4 units. The phase transition into the IC phase is of second order, but the lock-in transition into the spin-Peierls distortion below 74.5 K is of weak first order in nature.

DOI: 10.1103/PhysRevB.88.184420 PACS number(s): 61.44.Fw, 61.50.Ks, 64.70.Rh, 75.30.Kz

I. INTRODUCTION

The complex interplay between spin, charge, orbital, and lattice degrees of freedom has made low-dimensional quantum spin magnets with strong antiferromagnetic (AF) spin-exchange coupling prime candidates for studying unusual magnetic ground states.[1,2] For instance, a progressive spin-lattice dimerization in one-dimensional AF Heisenberg chains, which occurs below a critical temperature and induces a singlet ground state with a magnetic gap, is commonly referred to as spin-Peierls (SP) transition.[3] Such a transition, first observed in organic materials[4–6] attracted renewed attention when the first inorganic SP system, $CuGeO_3$ with Cu^{2+} spin $S = 1/2$ entities ($T_{SP} \sim 15$ K), was discovered about two decades ago.[7] The critical temperature of SP systems is essentially proportional to the intrachain spin-exchange interaction, J.[8] The search for systems with even higher SP transition temperatures focused on systems with one electron occupying the $3d$ shell, e.g., systems containing Ti^{3+} cations because the larger extension of their magnetic orbitals provides enhanced orbital overlap between adjacent sites. In addition, the weak spin-orbit coupling of these cations allows their spin exchange interactions to be well described by a Heisenberg Hamiltonian hence enabling comparisons with standard theory.[4,5,8]

Recently, the compounds TiOX (X = Cl, Br) have been intensively investigated due to their unconventional magnetic and structural properties.[9–16] Unlike standard SP systems, TiOCl and TiOBr showed two successive phase transitions at remarkably high temperatures. Upon cooling a continuous transition is observed at 90 K in TiOCl from the room-temperature phase to an incommensurate (IC) phase, which is followed by a first-order lock-in transition at 67 K into a commensurate SP phase.[12,14–17] X-ray diffraction studies found a Ti–Ti dimerization along the ribbon chains, which indicates direct exchange interactions between spins of neighboring Ti ions.[12] However, due to the two-dimensional character of the TiOX crystal structure, questions about the strength of the interchain spin-exchange interactions and their involvement in causing two successive transitions remained unanswered.[17]

Based on magnetic susceptibility, heat capacity and nuclear magnetic resonance (NMR) measurements, Law *et al.*[18] lately reported an apparently similar SP scenario with two transitions at $T_{c1} = 74$ K and $T_{c2} = 111$ K for titanium orthophosphate $TiPO_4$, containing Ti^{3+} cations with a $3d^1$ electronic configuration. $TiPO_4$ belongs to the rich family of $CrVO_4$-type oxides, which exhibit a wide range of different magnetic properties.[19–25] Compared to the TiOX compounds, $TiPO_4$ exhibits a significantly less complex crystal structure characterized by edge-sharing TiO_6 octahedra forming slightly corrugated TiO_2 ribbon chains which are interconnected by sharing corners with PO_4 tetrahedra (see Fig. 1).[26,27] The high-temperature magnetic susceptibility of $TiPO_4$ follows very well that of a $S = 1/2$ Heisenberg chain with a remarkably large nearest-neighbor AF spin-exchange constant of 965 K, about 50% larger than those of the TiOX compounds. DFT calculations indicated the interchain spin exchange to be less than 2% of the intrachain interaction and ESR measurements revealed the anisotropy of the g factor to be of the order of 1%.[28] Low-temperature susceptibility data showed a nonmagnetic singlet ground state.[18]

Based on ^{31}P NMR measurements, the low-temperature phase ($T < T_{c1}$) was ascribed to a commensurate phase with a Ti–Ti bond alternation along the Ti chains, generating two different P positions. In the intermediate phase, the NMR experiments found a broad asymmetric continuum characteristic for an IC phase.[18]

Here we report the discovery of the low-temperature superstructures of $TiPO_4$ by means of temperature-dependent x-ray diffraction experiments. Our measurements provide structural proof for an SP distortion, i.e., a Ti–Ti dimerization along TiO_2 ribbon chains parallel to **c**. In the intermediate phase, the crystal structure is IC and is characterized by a temperature-dependent modulation of the atom positions with a propagation **q** vector along $\mathbf{a}^*$. The complete accurate structural analysis, supported by density functional calculations, allowed to select the most favorable structural model for the low-temperature phase and to uncover the origin of the IC phase.

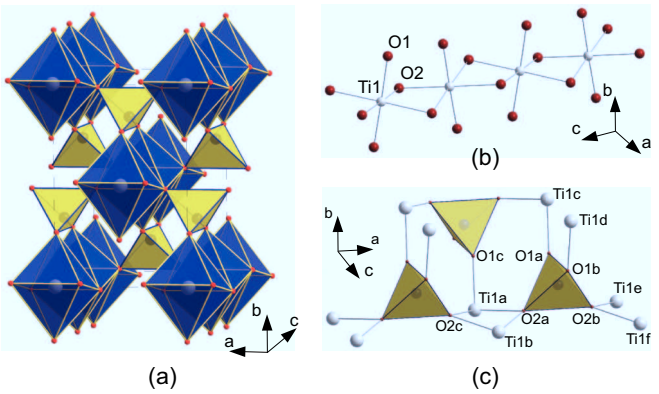

FIG. 1. (Color online) (a) Room-temperature crystal structure of $TiPO_4$ with *Cmcm* space group. (b) Chain of edge-sharing TiO_6 octahedra along **c**. (c) Fragment of the crystal structure showing interchain connections through PO_4 tetrahedral groups.

II. EXPERIMENTAL

Temperature-dependent single-crystal x-ray diffraction experiments on a high-quality single crystal of $TiPO_4$ were carried out using synchrotron and laboratory-based radiation sources.[29] Systematic **q** scans along all principal reciprocal lattice axes and diagonals at 10 K revealed superstructure reflections at positions $(h+\frac{1}{2},k,l)$, which can be indexed by a propagation vector $\mathbf{q}=(\sigma_1, 0, 0)$, where σ_1 amounts to $\frac{1}{2}$. Several strong superlattice satellite reflections were selected and their positions and integrated intensities were measured as a function of temperature. Their indices are independent of temperature up to 74 K, i.e., $\sigma_1=\frac{1}{2}$. At $T_{c1}=75$ K σ_1 exhibits a discontinuous jump to 0.527 and increases smoothly to 0.565 up to 110 K. Concomitantly, the satellites decrease their intensity and finally disappear at 112 K (see Fig. 2). These results show that below T_{c1} $TiPO_4$ forms a superstructure with a doubling of the room-temperature unit cell along **a**, whereas the crystal structure of the intermediate phase is incommensurately modulated. The discontinuity in σ_1 at T_{c1} [see Fig. 2(b)] indicates a weak first-order character of the phase transition, as is also supported by thermal hysteresis in the susceptibility and heat capacity measurements.[18] The smooth decrease of the satellite intensities on heating indicates a second-order phase transition at T_{c2}.

The change of length in dependence on temperature of an oriented single crystal (length ~1 mm) was followed by cooling and heating the sample with a miniature capacitance dilatometer.[29] Two phase transitions are also found in the thermal expansion data displayed in Fig. 3, then providing consistent transition temperatures of 74.9 and 112.5 K, respectively. The thermal hysteresis of *c* at T_{c1} (see lower inset on Fig. 3) without a sharp discontinuity again manifests the weak first-order nature of this transition. As also seen in temperature dependent x-ray diffraction data down to 100 K,[28] the length change with decreasing temperature of the lattice is distinctly anisotropic and characterized by an expansion upon cooling along **a** and **b** perpendicular to the Ti chains, whereas a contraction of the crystal along the Ti chains (along **c**) is observed.

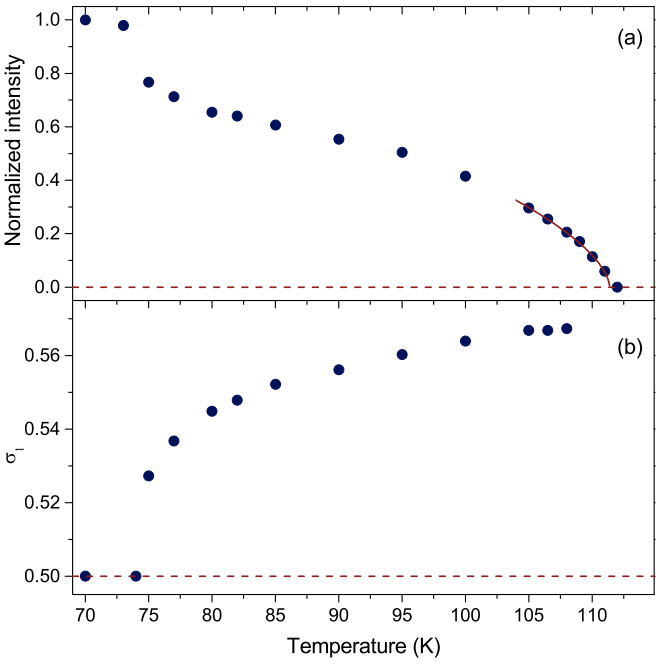

FIG. 2. (Color online) (a) Temperature dependence of the normalized intensities of the (2 4 3 −1) satellite Bragg reflection. The solid curve represents the fit with a critical power law with a critical temperature of $T_{c2}=111.6(3)$ K and a critical exponent of 0.32(2), consistent with standard universality classes. (b) Temperature dependence of the σ_1 component of $\mathbf{q}=(\sigma_1, 0, 0)$. Errors are smaller than the symbol sizes.

Two complete data sets of integrated intensities of Bragg reflections were collected at 10 and 82 K, corresponding to the commensurate and the IC phases, respectively. All observed Bragg reflections could be indexed with respect to the unit cell of the average structure and a modulation wave vector **q**, using four integers (*hklm*). This enables the use of the superspace approach for structural analysis, where the structural parameters are separated into the parameters of the

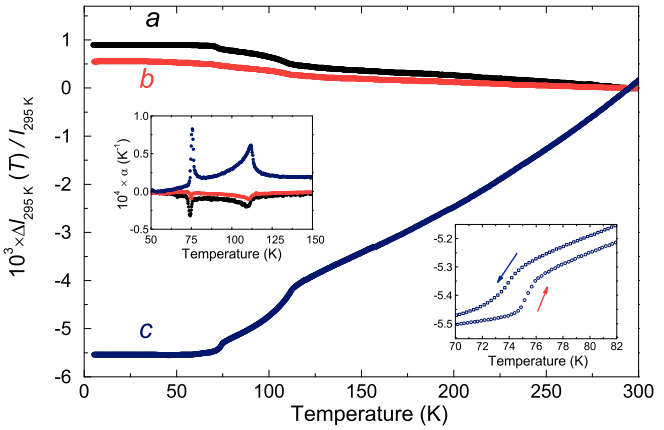

FIG. 3. (Color online) Relative length change (with respect to 295 K) of a single crystal of $TiPO_4$ along the three crystallographic directions as indicated. The upper inset displays the thermal expansion coefficients using the same color code. The lower inset magnifies the thermal hysteresis around the transition to the commensurate low-temperature phase.

average structure defined by main reflections ($m = 0$) and the modulation parameters defined by satellite reflections ($m \neq 0$).[30] The latter characterize relatively small displacements of the atoms, which can be described by a first-order Fourier series for the modulation functions:

$$u_i^{\mu}(\bar{x}_4) = A_i(\mu)\sin(2\pi\bar{x}_4) + B_i(\mu)\cos(2\pi\bar{x}_4), \qquad (1)$$

for $i = x$, y, and z. μ indicates the atom Ti, P, O1 or O2 in the average-structure unit cell, and $\bar{x}_4 = t + \mathbf{q}\cdot\bar{\mathbf{x}}$, where $\bar{\mathbf{x}}$ is the atomic position in the average structure. The parameter t represents the phase of the modulation.

It should be noted that no high-order satellites ($|m| > 1$) were observed at 10 K. The commensurate value of σ_1 at 10 K implies that the satellites with $|m| = 2$ would appear at the positions of the main reflections forbidden by the C centering of the lattice. No such reflections were detected during the data collection in the low-angle region up to $\sin(\theta)/\lambda < 0.31$ Å^{-1}. Therefore second-order reflections can be considered as absent in our experiment at 10 K, and these positions were excluded from the full data collection. No explicit search was performed for the second-order satellites at 82 K, mainly due to the beam-time limitations. Furthermore, in the IC phase at 82 K, reflections with $|m| = 1$ have $\langle I/\sigma(I)\rangle$ equal to 10.9 (compared to 200.8 for the main reflections). Therefore higher-order satellites, if any, are expected to be too weak to be observed in our experiment. The intensities of satellite reflections of order m are approximately proportional to the square of the amplitude of the m^{th}-order harmonic.[30] The absence of satellites with $|m| > 1$ implies that the modulation functions can be successfully described by exclusively first-order harmonics [see Eq. (1)]. All structure refinements were performed with standard software.[29]

Both low-temperature structures can be described by the same orthorhombic superspace group $Cmcm(\sigma_1 00)0s0$ [No. 63.1.13.8 with standard setting $Amam(00\sigma_3)0s0$].[31,32] In the description of the lock-in phase as commensurately modulated structure, different sections $t = t_0$ of superspace lead to different symmetries of the fourfold, $2a \times b \times c$ superstructure.[33] The best fit to the diffraction data was obtained for $t_0 = \frac{1}{8}$, which corresponds to space group $Pbnm$ for the superstructure [see Fig. 4(d)]. However, good agreement was also found for $t_0 = 0$, corresponding to space group $Pmnm$ [see Fig. 4(b)], and for $t_0 = \frac{1}{16}$, corresponding to the noncentrosymmetric space group $P2_1nm$ [see Fig. 4(c)].

III. DISCUSSION

The most prominent feature of the $Pbnm$ low-temperature superstructure is a dimerization of the Ti chains with a Ti–Ti bond alternation of about 3% [$d_1 = 3.134(5)$ and $d_2 = 3.230(5)$ Å] along **c**,[29] almost four times larger than that in $CuGeO_3$.[34] Compared to the room-temperature structure, the TiO_6 octahedra at 10 K are slightly more distorted, but they remain compressed with Ti–O distances to apical oxygen atoms (O1) clearly shorter than distances to equatorial oxygen atoms (O2). The Ti $3d$ orbitals are split into e_g and t_{2g} orbitals. With a coordinate system chosen as $z \parallel b$, $x \parallel a$, and $y \parallel c$, the

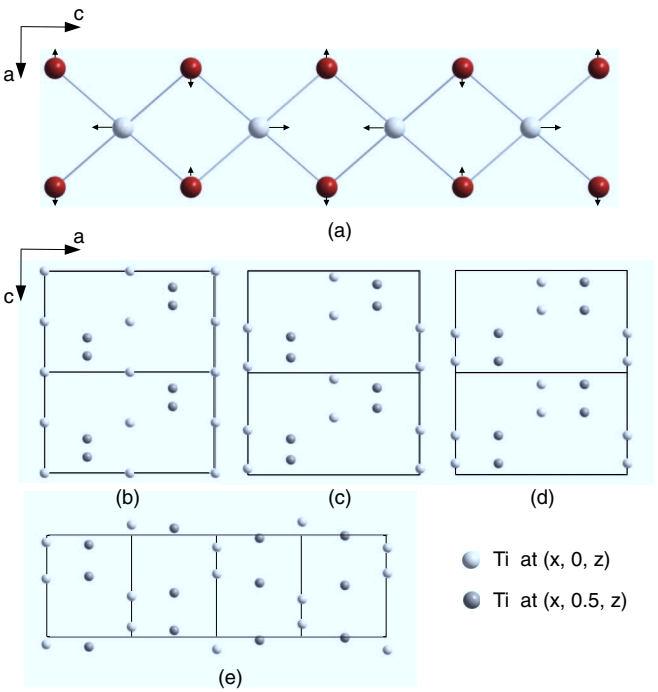

FIG. 4. (Color online) (a) Single TiO_2 chain from the crystal structure of $TiPO_4$. Arrows indicate the atomic displacements corresponding to the $Pbnm$ structure model for the spin-Peierls phase at 10 K. (b)–(d) Projection of the crystal structures at 10 K along [010]. (b) $2a \times b \times c$ supercells with $Pmnm$ symmetry, (c) with $P2_1nm$ symmetry, and (d) with $Pbnm$ symmetry. (e) Incommensurate phase at 82 K represented by $4a \times b \times c$ basic-structure unit cells. Only Ti atoms are shown. Basic-structure coordinates are $x = 0$ or $1/2$ and $z = 0$ or $1/2$. For clarity all atomic displacements have been multiplied by 30.

t_{2g} orbitals are further split into $d_{x^2-y^2}$ and almost degenerate d_{yz} and d_{xz}, the latter being higher in energy due to the compression of the TiO_6 octahedra.[35] The structure model thus is in agreement with direct magnetic exchange between unpaired electrons occupying the $d_{x^2-y^2}$ orbitals on Ti^{3+} atoms neighboring along **c**. While the displacements of Ti atoms are driven by SP coupling, the modulations of other atoms follow those of Ti to retain favorable bonding configurations. The latter is also implied by the negative thermal expansion along **a** and **b**. In the structure model described by the space group $Pmnm$ only Ti chains in every second layer undergo a dimerization [see Fig. 4(b)], in disagreement with the magnetic susceptibility data showing a nonmagnetic singlet ground state below T_{c1}.[18] The structure model $P2_1nm$ [see Fig. 4(c)] exhibits varying Ti–Ti dimerizations generating a total of four different P atoms. However, since the positional parameters of two pairs of P atoms are only marginally different,[29] this finding is at first hand not inconsistent with the NMR data detecting only two ^{31}P lines.[18]

In order to find the relative energies of these three putative low-temperature structures, density functional theory (DFT) electronic band structure calculations were carried out by employing the Vienna *ab initio* simulation package[36–38] with the projected augmented wave method and the generalized gradient approximation (GGA) for the exchange and the correlation functional.[39] To account for the electron correlation

TABLE I. Relative energies of the three possible low-temperature structures ($T < 75$ K) obtained from DFT + U calculations.

U (eV)	$Pbnm$ (meV)	$P2_1nm$ (meV)	$Pmnm$ (meV)
2	0	0.43	0.56
3	0	0.43	0.57

associated with the Ti $3d$ state, we performed DFT plus on-site repulsion (DFT + U) calculations[40] with an effective $U_{\text{eff}} = U - J = 2$ and 3 eV on Ti. Details of the calculations can be found in Ref. 29. The DFT calculations clearly identify the $Pbnm$ model as the structure with minimum energy (see Table I), supporting the results of the structure refinements. The two other structure models, however, are surprisingly close in energy, with consequences for the IC phase (see below).

A peculiarity of $TiPO_4$ is that a dimerization of the Ti chains along **c** is brought about by a doubling of the unit cell along **a**. This feature is explained by the loss of point symmetry accompanying the loss of translational symmetry, and the fact that the basic structure already contains two Ti atoms within one period along **c**. The IC phase at intermediate temperatures is characterized by an IC modulation along **a** as defined by $\mathbf{q} = (\sigma_1, 0, 0)$ (see Fig. 2). In the absence of a nonzero component along $\mathbf{c}^*$, the Ti chains along **c** remain dimerized, but chains centered at different x possess different degrees of dimerization [see Fig. 4(e)]. Some chains appear similarly dimerized as those in the low-temperature $Pbnm$ structure, while other chains are more like those in the $P2_1nm$ or $Pmnm$ low-temperature structures [compare Figs. 4(b)–4(e)]. In this respect, the IC structure of $TiPO_4$ is essentially different from the IC structure of TiOCl. An incommensurate component of the **q** vector along the chain direction in TiOCl determines that all chains are identically modulated in TiOCl, whereas the zero component of the **q** vector along the chain direction makes all chains differently dimerized in the IC structure of $TiPO_4$.

Since DFT calculations have revealed that the different models for the low-temperature crystal structure exhibit only small differences in energy (see Table I), we propose that the IC phase should be considered as a combination of all possible low-temperature structures. Fluctuations between energetically almost degenerate structures with different P environments allow one to understand the very broad ^{31}P NMR continuum in the IC phase spreading out over more than 200 ppm. In the commensurate phase below T_{c1}, the NMR spectrum contracts to two very sharp resonance lines separated by only ~5 ppm.[18] The dilatometry experiments revealed a negative thermal expansion perpendicular to the Ti chains, whereas a contraction of the lattice of significantly larger magnitude is seen along **c** (see Fig. 3). These findings indicate that elastic interactions mediated by the PO_4 units have to be considered between neighboring chains, in addition to the displacements of the Ti atoms driven by the SP dimerization.

The variation of a structural parameter (e.g., interatomic distances or bond angles) within the IC structure is given by a t-plot. The latter gives the value of this parameter as a function of the phase t of the periodic modulation wave.[30] An extended discussion of the t plots is given in Ref. 29. Selected t plots are presented in Fig. 5. Expectedly, the largest variation holds for Ti-Ti intrachain distances [see Fig. 5(a)], while the small

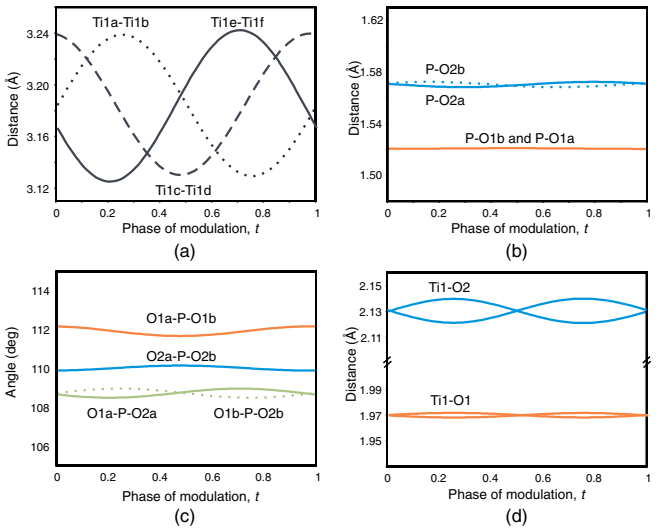

FIG. 5. (Color online) Selected t-plots for the IC phase at 82 K. Atom labels refer to the Fig. 1.

variations of P–O distances and O–P–O bond angles in the IC structure [see Figs. 5(b) and 5(b)] demonstrate that the PO_4 tetrahedra behave to a large extent as rigid units. On the other hand, the apical oxygen atoms of the TiO_6 octahedra (O1 in Fig. 1) follow and adjust to the SP dimerization of the Ti atoms, so that Ti–O1 distance variation is very small [see Fig. 5(d)]. Consequently, the shifts of the apical oxygen atoms will also affect the adjustment of the equatorial oxygen atoms (O2 atoms in Fig. 1) of TiO_6 octahedra in neighboring chains. The competition and frustration of the SP distortion in neighboring Ti chains, mediated by the elastic coupling by rigid PO_4 units, can explain the structural fluctuations in the IC phase indicated by the NMR experiment.

The proposed IC model also explains the behavior of the magnetic susceptibility reported in Ref. 18. The formation of spin-singlets starts below T_{c2}, and expectedly results in the drop of the magnetic susceptibility. Between T_{c2} and T_{c1} χ is defined by the nondimerized and slightly dimerized spin chains. As evidenced by the gradual rise of satellite intensities on further cooling [see Fig. 2(a)], the modulation amplitudes increase, and, therefore, the number of weakly dimerized chains decreases. Such chains disappear below T_{c1}, resulting in almost zero magnetic susceptibility in the lock-in phase.

IV. CONCLUSIONS

In conclusion, $TiPO_4$ shows a SP phase below $T_{c1} = 74$ K, that is characterized by a dimerization of the Ti chains along **c**. The occurrence of an IC phase extending up to temperatures significantly above T_{c1} is unexpected within a standard SP scenario. The IC phase is ascribed to energetically almost degenerate phases resulting from a competition and frustration of the SP transition due to elastic coupling between neighboring Ti chains. The transitions between the different phases involve sizeable lattice anomalies with a contraction of the lattice along the spin chains whereas perpendicular to the Ti chains an expansion of the lattice is found.

ACKNOWLEDGMENTS

We thank M. Tolkiehn for his assistance with the synchrotron experiment at beamline D3 of Hasylab at DESY in Hamburg, Germany. Financial support by the German Science Foundation (DFG) is gratefully acknowledged. MHW thanks the HPC Center of NCSU and the NERSC Center for computing resources.

*smash@uni-bayreuth.de

[1]E. Dagotto, Science **309**, 257 (2005).
[2]P. A. Lee, Rep. Prog. Phys. **71**, 012501 (2008).
[3]A. I. Buzdin and L. N. Bulaevskii, Sov. Phys. Usp. **23**, 409 (1980).
[4]J. W. Bray, J. H. R. Hart, L. V. Interrante, I. S. Jacobs, J. S. Kasper, G. D. Watkins, S. H. Wee, and J. C. Bonner, Phys. Rev. Lett. **35**, 744 (1975).
[5]I. S. Jacobs, J. W. Bray, H. R. Hart, L. V. Interrante, J. S. Kasper, G. D. Watkins, D. E. Prober, and J. C. Bonner, Phys. Rev. B **14**, 3036 (1976).
[6]B. van Bodegom, B. C. Larson, and H. A. Mook, Phys. Rev. B **24**, 1520 (1981).
[7]M. Hase, I. Terasaki, and K. Uchinokura, Phys. Rev. Lett. **70**, 3651 (1993).
[8]E. Pytte, Phys. Rev. B **10**, 4687 (1974).
[9]A. Seidel, C. A. Marianetti, F. C. Chou, G. Ceder, and P. A. Lee, Phys. Rev. B **67**, 020405(R) (2003).
[10]T. Saha-Dasgupta, R. Valentí, H. Rosner, and C. Gros, Europhys. Lett. **67**, 63 (2004).
[11]L. Pisani, R. Valentí, B. Montanari, and N. M. Harrison, Phys. Rev. B **76**, 235126 (2007).
[12]M. Shaz, S. van Smaalen, L. Palatinus, M. Hoinkis, M. Klemm, S. Horn, and R. Claessen, Phys. Rev. B **71**, 100405(R) (2005).
[13]L. Palatinus, A. Schönleber, and S. van Smaalen, Acta Crystallogr. C **61**, i47 (2005).
[14]A. Schönleber, S. van Smaalen, and L. Palatinus, Phys. Rev. B **73**, 214410 (2006).
[15]A. Schönleber, G. Shcheka, and S. van Smaalen, Phys. Rev. B **77**, 094117 (2008).
[16]S. van Smaalen, L. Palatinus, and A. Schönleber, Phys. Rev. B **72**, 020105(R) (2005).
[17]R. Rückamp, J. Baier, M. Kriener, M. W. Haverkort, T. Lorenz, G. S. Uhrig, L. Jongen, A. Möller, G. Meyer, and M. Grüninger, Phys. Rev. Lett. **95**, 097203 (2005).
[18]J. M. Law, C. Hoch, R. Glaum, I. Heinmaa, R. Stern, J. Kang, C. Lee, M.-H. Whangbo, and R. K. Kremer, Phys. Rev. B **83**, 180414(R) (2011).
[19]R. Glaum, M. Reehuis, N. Stüßer, U. Kaiser, and F. Reinauer, J. Solid State Chem. **126**, 15 (1996).
[20]J. P. Wright, J. P. Attfield, W. I. F. David, and J. B. Forsyth, Phys. Rev. B **62**, 992 (2000).
[21]J. P. Attfield, P. D. Battle, and A. K. Cheetham, J. Solid State Chem. **57**, 357 (1985).
[22]P. D. Battle, T. C. Gibb, G. Hu, D. C. Munro, and J. P. Attfield, J. Solid State Chem. **65**, 343 (1986).
[23]M. J. Isasi, R. Sáez-Puche, M. L. Veiga, C. Pico, and A. Jerez, Mater. Res. Bull. **23**, 595 (1988).
[24]H.-J. Koo, M.-H. Whangbo, and K.-S. Lee, Inorg. Chem. **42**, 5932 (2003).
[25]J. M. Law, P. Reuvekamp, R. Glaum, C. Lee, J. Kang, M.-H. Whangbo, and R. K. Kremer, Phys. Rev. B **84**, 014426 (2011).
[26]N. Kinomura, F. Muto, and M. Koizumi, J. Solid State Chem. **45**, 252 (1982).
[27]R. Glaum and R. Gruehn, Z. Kristallogr. **198**, 41 (1992).
[28]J. M. Law, Ph.D. thesis, Loughborough University, Loughborough, UK, 2011.
[29]See Supplemental Material at http://link.aps.org/supplemental/10.1103/PhysRevB.88.184420 for more details of the experimental procedures.
[30]S. van Smaalen, *Incommensurate Crystallography* (Oxford University Press, Oxford, 2007).
[31]H. T. Stokes, B. J. Campbell, and S. van Smaalen, Acta Crystallogr. A **67**, 45 (2011).
[32]S. van Smaalen, B. J. Campbell, and H. T. Stokes, Acta Crystallogr. A **69**, 75 (2013).
[33]Note that doubling of the *a* axis together with loss of the *C* center imply that the volume of the primitive unit cell is increased by a factor of four. Therefore the superstructure is a fourfold superstructure.
[34]M. Braden, G. Wilkendorf, J. Lorenzana, M. Aïn, G. J. McIntyre, M. Behruzi, G. Heger, G. Dhalenne, and A. Revcolevschi, Phys. Rev. B **54**, 1105 (1996).
[35]R. Glaum and M. A. Hitchman, Aust. J. Chem. **49**, 1221 (1996).
[36]G. Kresse and J. Hafner, Phys. Rev. B **47**, 558 (1993).
[37]G. Kresse and J. Furthmüller, Comput. Mater. Sci. **6**, 15 (1996).
[38]G. Kresse and J. Furthmüller, Phys. Rev. B **54**, 11169 (1996).
[39]J. P. Perdew, K. Burke, and M. Ernzerhof, Phys. Rev. Lett. **77**, 3865 (1996).
[40]S. L. Dudarev, G. A. Botton, S. Y. Savrasov, C. J. Humphreys, and A. P. Sutton, Phys. Rev. B **57**, 1505 (1998).